PHYSICAL REVIEW E **68**, 056408 (2003)

Spatial characteristics of Kα x-ray emission from relativistic femtosecond laser plasmas

Ch. Reich, I. Uschmann, F. Ewald, S. Düsterer, A. Lübcke, H. Schwoerer, R. Sauerbrey, and E. Förster
Institut für Optik und Quantenelektronik, Friedrich-Schiller-Universität Jena, Max-Wien-Platz 1, D-07743 Jena, Germany

P. Gibbon
John von Neumann Institute for Computing, ZAM, Forschungszentrum Jülich GmbH, D-52425 Jülich, Germany

(Received 30 April 2003; revised manuscript received 30 July 2003; published 21 November 2003)

The spatial structure of the Kα emission from Ti targets irradiated with a high intensity femtosecond laser has been studied using a two-dimensional monochromatic imaging technique. For laser intensities $I < 5 \times 10^{17}$ W/cm^2, the observed spatial structure of the Kα emission can be explained by the scattering of the hot electrons inside the solid with the help of a hybrid particle-in-cell/Monte Carlo model. By contrast, at the maximum laser intensity $I = 7 \times 10^{18}$ W/cm^2 the half-width of the Kα emission was 70 μm compared to a laser-focus half-width of 3 μm. Moreover, the main Kα peak was surrounded by a halo of weak Kα emission with a diameter of 400 μm and the Kα intensity at the source center did not increase with increasing laser intensity. These three features point to the existence of strong self-induced fields, which redirect the hot electrons over the target surface.

DOI: 10.1103/PhysRevE.68.056408 PACS number(s): 52.38.Fz, 52.38.Ph, 52.59.Px

I. INTRODUCTION

High intensity, femtosecond lasers are now routinely used to produce energetic particles and photons via their interaction with solid targets [1]. In particular, the suprathermal electrons generated near the target surface can be exploited to produce short-pulse, characteristic Kα radiation as they penetrate the cold bulk material inside. Since the hot electrons are only produced during the laser irradiation, Kα sources with sizes comparable to the laser focus size [2,3] and femtosecond duration [4–6] can in principle be realized. Such x-ray sources have high potential for applications in time-resolved x-ray diffraction [7,8] and medical imaging [9,10], both of which depend critically on the source size to achieve high spatial resolution and contrast.

A widely used method to measure the size of the Kα emission from a laser-produced plasma is one-dimensional x-ray shadowgraphy at a knife edge [11]. In this technique the x-ray intensity is spatially integrated parallel to the knife edge. Nevertheless, the $1/e$ width of a Gaussian x-ray source is retained in the integration, so that the method is widely used to estimate the half-width of laser plasma Kα sources [2,3,11–15].

The spatial distribution of the Kα emission reflects the trajectories of the hot electrons, along which the Kα photons are generated. In a simplified description the electron dynamics can be reduced to two stages: the generation of the hot electrons in the plasma and the scattering of the electrons in the solid. The electrons are assumed to move in a straight line from the acceleration point to the solid, and in the simplest modeling each electron enters the solid perpendicular to the surface. In a more sophisticated modeling the conservation of momentum between the laser photons and the generated hot electron is taken into account, with the consequence that the electron enters the solid in a direction, which depends on its energy: for low electron energies the electron moves in the direction of the target normal, for high energies in that of the laser beam [16–19]. Thus, the Kα source size is determined by the extension of the laser focus and by the lateral scattering of the hot electrons inside the solid.

The numerical implementation of such a model can be realized by combining a particle-in-cell (PIC) code for the laser absorption with a Monte Carlo (MC) code for the subsequent generation of Kα radiation in a solid. We have previously applied this model to calculate the yield ratios from multilayer targets and to estimate hot electron temperatures from femtosecond laser-solid interactions [20].

Recently Eder *et al.* [12] estimated the size and the total yield of a Cu Kα source in the intensity range 5×10^{15}–2×10^{18} W/cm^2 by knife-edge measurement. Combining a Monte Carlo electron transport code with a simple scaling law for the hot electron temperature, they were able to reproduce the total Kα yield for the different laser intensities, but predicted much smaller source sizes than measured, implying that additional mechanisms were affecting the electron transport. One possibility is that the hot electrons perform complex orbits in self-generated electric and magnetic fields in front of the target before they enter into the solid [12,21]. Such behavior was studied 20 years ago for solid targets irradiated by the laser systems at that time ($I = 10^{14} - 10^{16}$ W/cm^2 and pulse durations of several 10 to 100 ps) [22–24]. Another possibility is that the hot electrons do not enter the solid unidirectionally but with some angular spread. Authors who studied the size of the Kα emission from fluorescence layers buried behind another material found that the measured Kα emission sizes and their dependence on target depth can be reproduced by assuming that the hot electron beams have half-cone angles between 15° and 90° [13–15]. These observations contradict the theoretical considerations on the hot electron entrance angle mentioned above, and pose the question how the hot electrons achieve such an angular spread.

For high laser intensities ($I > 10^{17}$ W/cm^2) a general picture is thus beginning to emerge in which Kα source sizes are found to be much larger than expected by simple modeling. It is therefore natural to ask *where* the Kα emission

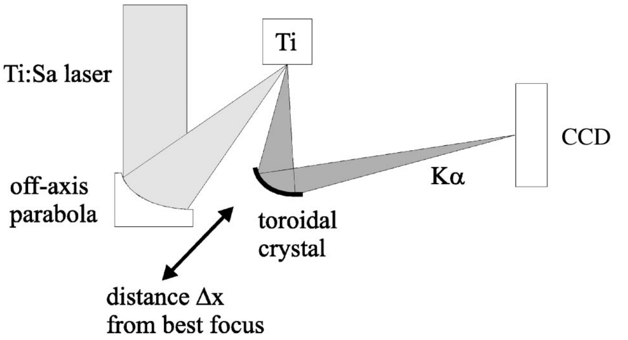

FIG. 1. Scheme of the experimental setup. The Kα emission was imaged via a toroidally bent Si(311) crystal onto a CCD camera. The maximum laser intensity was 7×10^{18} W/cm^2 with a focus size of 3 μm.

actually originates under these conditions.

In the present paper we present the systematic study of the spatial distribution of the Kα radiation from a laser plasma source. The Kα emission from laser-irradiated bulk Ti targets was measured with two-dimensional resolution, using a toroidally bent crystal as the imaging x-ray optics. The laser parameters and the imaging properties of the crystal were carefully determined, so that the experimental situation could be reproduced with high accuracy by a PIC-MC simulation model. For low laser intensities ($I=3\times10^{16}$ W/cm^2), the simulations proved to be in agreement with the measurements. At high intensities ($I=7\times10^{18}$ W/cm^2), distinct deviations in the spatial distribution between the modeling and the measurements occurred, indicating that self-induced fields have played an important role in our experiment.

II. EXPERIMENTAL SETUP

The experiment (Fig. 1) was performed with the Jena Ti:sapphire laser ($\lambda=800$ nm, pulse duration 90 fs), which delivered an energy of 240 mJ onto a bulk Ti target. The laser was focused with an off-axis parabola ($f=120$ mm), giving a half-width of 2×4 μm^2 at best focus (Fig. 2). The intensity distribution of the laser focus was measured with a microscope and a charge-coupled device (CCD) camera. A dynamic range of 10^3 was achieved by superimposing two CCD images, taken with and without gray filters in front of the camera. These images were taken at the same laser energy as used for the measurements and with an attenuator being introduced into the laser beam in front of the compressor. It was checked that the attenuator did not affect the beam profile. The nominal laser intensity was identified with the mean intensity in the area, where the laser intensity was above $1/e$ of its maximum value. At best focus the nominal laser intensity was 7×10^{18} W/cm^2 and 47% of the laser energy was within the $1/e$ width.

The laser was defocused by moving the parabola along the focal axis toward the target or away from it. The intensity distribution of the focus was measured in a defocus range -400 μm$\leqslant\Delta x\leqslant+400$ μm, limited by the size of the focus image on the CCD camera. At a defocus distance of $|\Delta x|=400$ μm the nominal laser intensity was $3-5\times10^{16}$ W/cm^2. To estimate the laser intensity at greater defocusing distances the laser intensity profile was approximated by a Gaussian profile with a half-width of 3 μm at best focus.

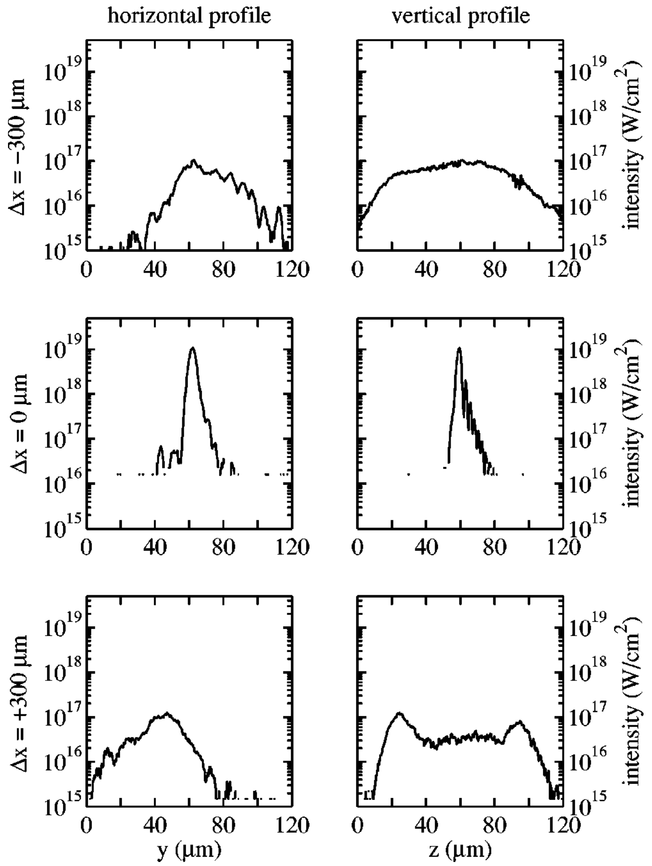

FIG. 2. Laser beam profiles at different distances Δx from the best focus position.

The laser was p polarized and the angle of incidence was 45°. The temporal shape of the laser pulse was measured with a third-order multishot autocorrelator. The pulse duration (full width at half maximum) was 90 fs. Two intrinsic prepulses were found with intensity contrast ratios of 3×10^{-4} and 3×10^{-3} at 4 ps and 600 fs before the main pulse, respectively.

The Ti target was polished to ensure a good shot-to-shot reproducibility. After each shot, the target was moved 500 μm to an unused part.

A toroidally bent Si(311) crystal delivered a two-dimensional, magnified image of the Kα emission onto a CCD camera [25,26]. A magnification of 7 was used, which gave together with the CCD pixel size of 21 μm a resolution of 6 μm. Each Kα photon reflected by the crystal onto the CCD corresponded to 2.1×10^5 photons emitted from the target in 1 sr. A similar imaging was performed for the Kα emission from the target side perpendicular to the laser irradiated side. The results of this imaging were published elsewhere [27].

The x-ray images delivered by the bent crystal differ from the true shape of the Kα emission due to aberrations. The influence of the aberrations for the experimental conditions was studied at an x-ray tube and via ray tracing. It was found that a sharp edge of the x-ray source is broadened to $\sim 10\ \mu$m in the image. As the experimental Kα emission does not have a sharp edge but decreases continuously towards the borders, ray-tracing calculations for a Kα source with a Gaussian shape were performed. It was found that in the direction perpendicular to the dispersion plane the shape and size of such a source are preserved. In the results section the extension of the Kα images in this direction is used to estimate the half-width of the Kα emission. In the direction of the dispersion plane the half-width of a Gaussian source experiences a broadening, which depends on the source size. The broadening is ~ 2 for a source size of 5 μm and ~ 1.2 for 50 μm.

From the Kα images the properties of the corresponding Kα sources were derived, such as the total Kα yield, the spatial half-width, and the Kα intensity at the source center. Two sources of error were taken into account: the noise of the CCD camera and the uncertainty of where exactly the source center is. The noise of the camera was estimated from a part of the images, which was far away from the Kα signal. From that error bars for the total Kα yield were derived. A range for the position of the source center was estimated by taking the 20 CCD pixels with the highest Kα signals as possible candidates. The range of half-widths corresponding to these pixels was then used as error bars for the half-width of the Kα source. Finally, for the error bars of the central Kα emission both the camera noise and the standard deviation of the 20 pixels with the highest Kα signals were taken into account.

III. MODELING OF THE Kα EMISSION

A combined PIC-MC simulation model was used to calculate spatially resolved Kα emissions. The simulation model uses the one-and-a-half-dimensional oblique incidence, particle-in-cell code BOPS [28,29] with one space coordinate (parallel to the target normal) and two velocity components [parallel (v_x) and perpendicular (v_y) to the target normal]. Oblique incidence of the laser is handled via the boost frame method. The calculations were performed for the experimental laser parameters given in the preceding section. An exponentially decreasing plasma density with a normalized scale length $L/\lambda = 0.3$ was used, appropriate to the preformed plasma generated by the experimental prepulses [30]. The maximum plasma density was $10n_c$ with n_c being the critical density.

A phase space of the generated hot electrons as calculated by the PIC code is shown in Fig. 3. The ratio of the components of the hot electron momenta p_y/p_x gives the simulated entrance angles of the electrons. The PIC simulations reproduce the theoretical energy dependence [16,17] with the low energy electrons moving parallel to the target normal while the high energy electrons enter in the direction of the laser beam.

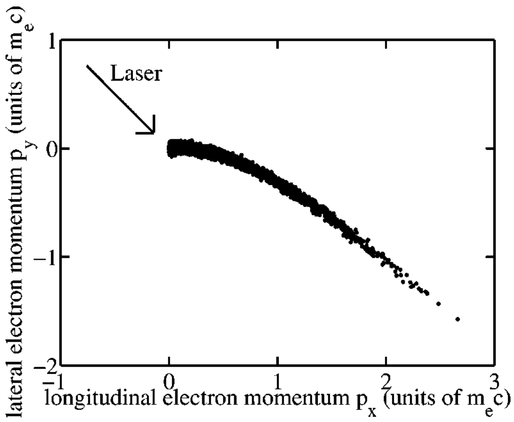

FIG. 3. Direction of the generated hot electrons for a laser intensity of 3×10^{17} W/cm^2 as simulated with the PIC code.

The energy distributions of the hot electrons simulated by the PIC code show a bi-Maxwellian shape as it was also found in experiments [31,32,14] and further PIC simulations [14,20,33]. We find a temperature scaling of the "hotter" part of the electron spectrum according to

$$T_{hot} \approx 110 \left(\frac{I\lambda^2}{10^{17}\ \mathrm{W\,cm^{-2}}\ \ \mu\mathrm{m}^2} \right)^{1/2} \ \mathrm{keV}. \qquad (1)$$

This scaling of the hot electron temperature with irradiance ($I\lambda^2$) agrees with the values given in the literature, where a dependence of $T_{hot} \propto (I\lambda^2)^{1/3,\ldots,1/2}$ is found [1]. The absolute values of T_{hot} given by Eq. (1) agree within a factor of 0.3, . . . ,2 with the hot electron temperatures found in recent experiments [14,31,32].

The scattering of the hot electrons in the solid and the Kα generation were simulated with a three-dimensional (3D) Monte Carlo code, which calculates the 2D distribution of the emitted Kα radiation. The code is extensively described in Ref. [27]. The accuracy of the MC simulations was checked by comparison with the experimental data on the Kα yield from monoenergetic electron beams penetrating into cold solids given by Dick *et al.* [34].

The simulation of the spatially resolved Kα emissions started with combined PIC-MC calculations for a range of laser intensities, giving the spatial Kα distributions resulting from pointlike laser spots [Fig. 4(a)]. Then, these Kα emissions were summed up according to the measured laser intensity distribution in the focus [Fig. 4(b)]. For the summation a grid of irradiated points within the focal area was used with each grid point representing an area $A = 1\ \mu\mathrm{m}^2$. This gives the calculated intensity distribution of the Kα source for the experimental laser conditions.

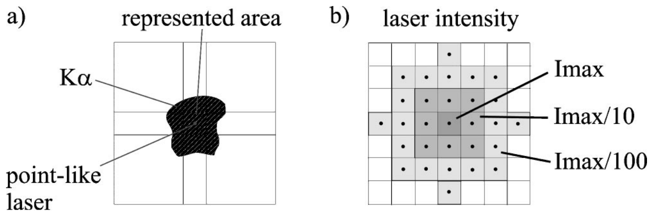

FIG. 4. Schematic illustration of calculating spatial Kα distributions: (a) Kα emission for a "pointlike" laser spot representing an irradiated area A. (b) Summation grid for a circular laser spot.

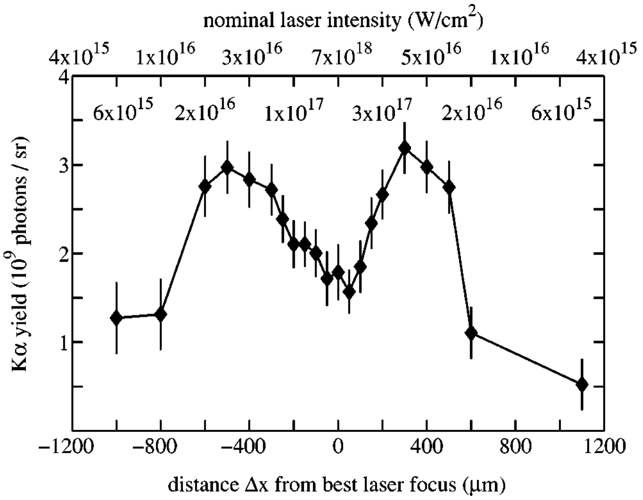

FIG. 5. Change of the total Kα yield when the laser is defocused. The Kα yield is maximum for a nominal laser intensity in the range 10^{16}–10^{17} W/cm^2. This is two orders of magnitude lower than the maximum laser intensity in the experiment.

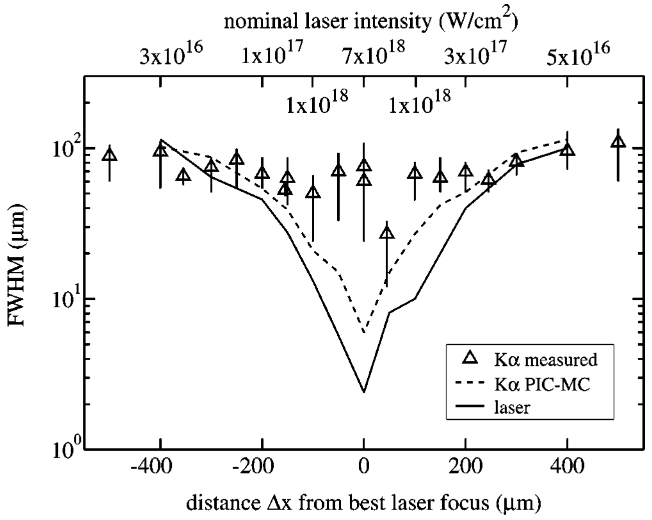

FIG. 6. Full width at half maximum of the laser focus, the measured and the simulated Kα emission depending on the distance from the best focus position. The half-width of the Kα source is basically constant at 70 μm. At the best focus it is 23 times larger than that of the laser focus.

To derive Kα images, which can be directly compared with the experimental images, the imaging process in the experiment was simulated with ray tracing [35] using the calculated x-ray emissions as an input.

IV. RESULTS

In the experiment, images of the Kα emission were taken for constant laser energy. By changing the distance Δx between the target and the best laser focus the intensity distribution in the focus was varied. The defocusing distance Δx was varied between ± 1100 μm.

The total Kα yield in these images shows a characteristic dependence on Δx with two maxima symmetrical around the highest laser intensity (Fig. 5). The yield maxima occur in the range $|\Delta x| \approx 300$–500 μm, which corresponds to a nominal laser intensity between 10^{16} and 10^{17} W/cm^2. This optimal laser intensity for Kα yield is two orders of magnitude lower than the laser intensity at the best focus position.

The Kα emission from the center of the Kα source shows a dependence on laser intensity which is similar to that of the total Kα yield, with maxima on both sides of the best focus position, but the variation is smaller than for the total yield.

The spatial half-width of the emission is basically independent of the laser focus size over the whole investigated defocus range (Fig. 6). It is about 70 μm, which is 23 times larger than the half-width of the best laser focus.

For the highest laser intensities, the Kα main peak is surrounded by a wide halo of weak Kα emission, which is only little above the noise level of the images. The size of the halo *increases* when the laser intensity is increased. At best focus, the halo has a diameter of 400 μm. In this case, two-thirds of the Kα emission come from outside the spatial half-width. This large extension of the Kα emission was also found in the imaging from the target side [27].

Kα emission profiles which resolve the intensity distribution in the halo were derived in two steps. First, the total Kα emission at a given distance from the focus center was found by angular integration of the Kα emission from concentric rings. Then, the integrated Kα emissions were normalized by the area of the corresponding ring. This procedure gave Kα emission profiles with a dynamic range of two orders of magnitude (Fig. 7). As the procedure is based on circular symmetry, the resulting Kα emission profiles are an average

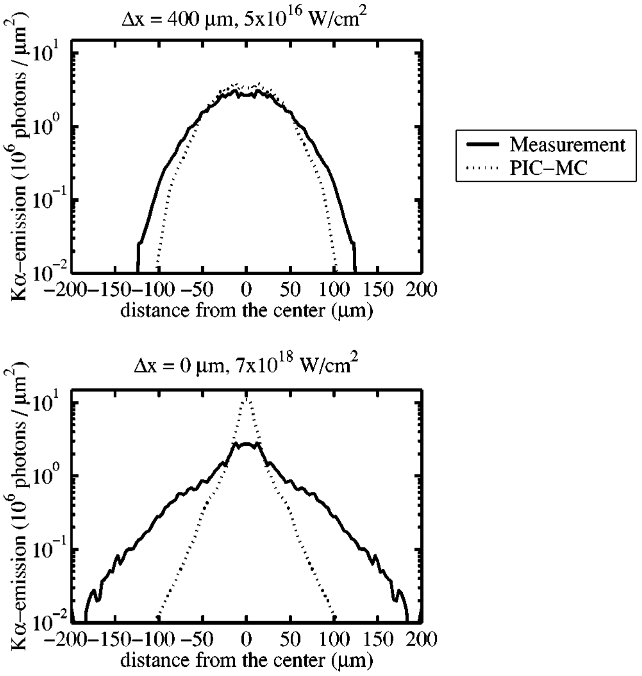

FIG. 7. Kα emission profiles for low ($I < 5 \times 10^{17}$ W/cm^2) and high laser intensities ($I > 5 \times 10^{17}$ W/cm^2). For low intensities the emission profile is reproduced by the PIC-MC simulations. For high intensities the central Kα emission is lower and the Kα source is larger than simulated.

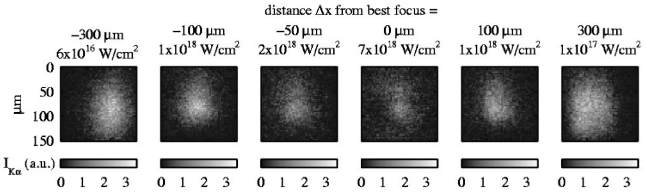

FIG. 8. Series of Kα images taken at different laser intensities. For the highest intensities ($I > 5 \times 10^{17}$ W/cm^2) the Kα emission from the center of the source is reduced compared to lower laser intensities.

of the emission profiles of all directions.

These profiles exhibit two distinct intensity regimes for the Kα emission. For laser intensities $I < 5 \times 10^{17}$ W/cm^2 the emission profile shows a superexponential dependence of the Kα emission on the distance from the emission center (Fig. 7, top). Thus, the emission consists of one broad peak. For high laser intensities ($I > 5 \times 10^{17}$ W/cm^2), the central Kα peak is surrounded by a weak halo with the Kα emission decreasing almost exponentially with distance from the emission center (Fig. 7, bottom). For these laser intensities, the Kα emission from the center of the source decreases with increasing laser intensity (Figs. 8, 7, and 10).

To compare the measured Kα images with the predictions of the simulation model, the intensities of the simulated images were normalized to the measured ones. For the images at $\Delta x = -400$ μm, the calculated Kα yield is 40% lower than measured while the relative distribution of the Kα emission is well reproduced. For the medium laser intensity at this defocus distance ($I = 3 \times 10^{16}$ W/cm^2) the influence of self-induced fields is expected to be negligible and the numerical model to be in agreement with the experiment. Therefore, the calculated $K\alpha$ emissions were normalized in such a way that the simulated and measured total Kα yields of the images at $\Delta x = -400$ μm are the same. With this normalization the simulation quantitatively reproduces the measured Kα distribution of this image. The difference in total Kα yield between simulation and experiment can be accounted for by the uncertainty in the experimental plasma parameters: a variation of the plasma density scale length L/λ of ± 0.1 can, for example, change the Kα yield by a factor of 2 or more [36].

The calculations reproduce the Kα emission profiles at low and moderate laser intensities (Fig. 7, top) as well as the dependence of the total Kα yield on laser intensity (Fig. 9). At high intensities the calculated emission profiles are very different from the measured ones (Fig. 7, bottom): the calculated Kα emission from the source center is several times higher than measured and the Kα halo is *completely absent* in the simulations.

V. DISCUSSION

A dependence of the total Kα yield on the defocus distance similar to that in Fig. 5 was also measured for Si [37], Cu [12], and Ti foil targets [38]. In a previous paper [4] we explain the existence of a Kα yield maximum by means of the reabsorption of Kα photons inside the target. At low laser intensities, the hot electron temperature is low, so that only few electrons have energies high enough to ionize the *K* shell of the target atoms. When the laser is focused to higher intensities, the hot electron temperature increases and more Kα photons are generated. At even higher laser intensities, the Kα yield decreases again, because the generated hot electrons now penetrate deeply beyond the Kα absorption length and most of the generated photons are reabsorbed on their way to the target surface.

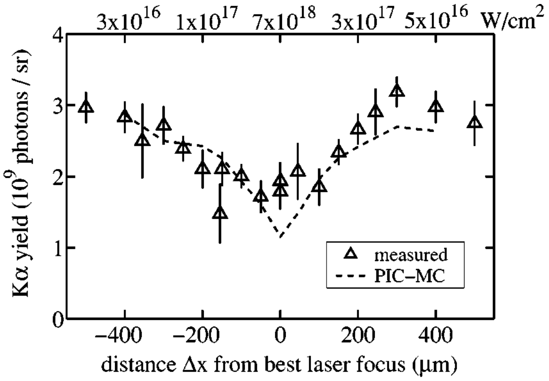

FIG. 9. Dependence of the total Kα yield on defocus distance (same data as in Fig. 5). The top axis shows the corresponding nominal laser intensities. The general tendency of the measured data is well reproduced by the simulations. For the highest laser intensities the measured Kα yield remains constant, while the simulations predict a decrease.

This explanation for the yield maximum with bulk targets is different from that for the Kα radiation from thin foils. Although reabsorption plays no role in thin foils, the Kα emission from such targets also shows a yield maximum at medium laser intensities, together with a second increase of the yield above intensities of 10^{18} W/cm^2. This intensity dependence results from the dependence of the *K*-shell ionization cross section on the energy of the hot electrons [38].

For bulk targets, Reich *et al.* [4] predict an optimal laser intensity of $I_{opt} = 10^{16}$ W/cm^2 for the generation of Ti Kα emission, which is at the lower limit of the measured optimum intensity range. The slight difference might be due to the approximation of the laser intensity distribution in the focus by a single nominal intensity. In PIC-MC simulations taking into account the full experimental laser beam profile the dependence of the Kα yield on the defocus distance and its two maxima are well reproduced (Fig. 9). The optimum laser intensity lies well within the low intensity domain, where the experimental behavior is reproduced by the numerical model.

When the laser is focused to higher intensities, the electron flux density increases. Therefore, the simulation model predicts that the number of Kα photons generated in the focus center increases (dashed line in Fig. 10). Such an increase of the peak Kα emission is *not* observed in the measurements. In fact, right at best focus, the central Kα emission even drops (triangles in Fig. 10).

The extension of the Kα source is expected to be larger than that of the laser focus due to the entrance angles of the hot electrons and their lateral scattering in the solid. To esti-

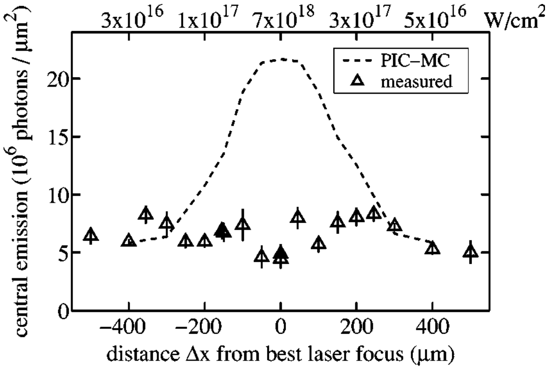

FIG. 10. Dependence of the Kα emission from the source center on defocus distance. The top axis shows the corresponding nominal laser intensities. For intensities above $\sim 10^{17}$ W/cm^2 the measured emission from the center of the source is several times lower than predicted by the simulations.

mate which relative broadening of the Kα source with respect to the laser focus can be expected due to these two factors, we performed a series of PIC-MC simulations for laser foci with Gaussian shapes, having different intensities and focus sizes. As stated in the numerics section, these simulations assume entrance angles of the hot electrons given by their energy (Fig. 3). We found that the relative broadening of the Kα emission area is less than a factor of 2 for any combination of laser intensity and focus size (Fig. 11). Here, "broadening" is defined as the ratio of the half-width of the Kα emission to that of the laser focus.

For higher laser intensities, the observed relative broadening of the Kα source is much larger than a factor of 2. The measured broadening is comparable to the experimental results by other authors, who found an increase of the relative broadening with increasing laser intensity, from a 1.5× broadening at 2×10^{16} W/cm^2 [2] over 3× at 5×10^{17} W/cm^2 [25] to 25× at 2×10^{19} W/cm^2 [15].

As mentioned in the Introduction, self-induced electric and magnetic fields are often invoked to explain measured Kα source sizes which are larger than can be explained solely by electron scattering in the solid. To gain insight, how these fields could affect the Kα emission, we estimated for our experimental conditions the shape and magnitude of three self-induced fields and how they influence the hot electron trajectories. We found that the interplay of these three fields modifies the calculated spatial Kα distribution into the direction of the experimental observations, such as lower peak Kα emission, greater half-width, and larger total extension of the source, thus, giving a better agreement between modeling and measurement than without these fields.

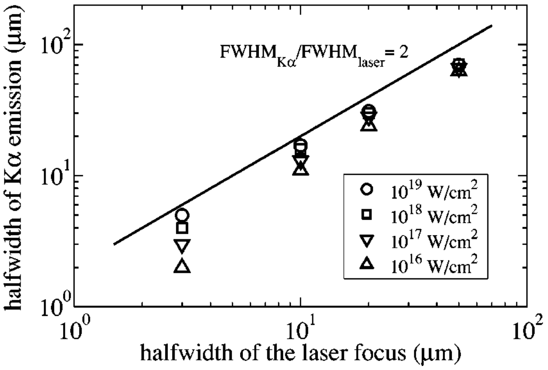

FIG. 11. Simulated spatial half-widths (full width at half maximum) of the Kα emission resulting from Gaussian laser foci with different sizes and intensities.

We took into account the ponderomotive field of the laser, the space charge field developing at the critical density, and the thermoelectric magnetic field generated by the noncollinear temperature and density gradients in the expanding plasma [39] created by the prepulses. We used an idealized focal spot with a Gaussian shape and a half-width of 3 μm and computed about 900 sample trajectories of hot electrons in the resulting fields. The resultant electron data were weighted by the hot electron distribution from the PIC simulations and again used as an input to the Monte Carlo transport code.

Hydrodynamic simulations using the MEDUSA code [40] suggest the presence of a thin magnetic field of several tens of megagausses situated between the critical plasma density and the solid. It was found that the lower energy fraction of the hot electrons was reflected by the magnetic field and prevented from entering the solid at the center of the laser focus. This reduces the central Kα emission by a factor of 4 compared to the calculations without field, which is similar to the reduction in the experiment. A similar reduction occurs even if saturation of the magnetic field [41] at a magnitude of several megagausses is taken into account.

The reflected electrons could then traverse the space charge field at the critical density and be distributed by the ponderomotive field of the laser. Both fields have similar maximum strengths of $\approx 2\times10^{12}$ V/m for our laser parameters. Since the ponderomotive field is also directed laterally, it can spread reflected hot electrons over a wider area of the target surface. Indeed, the half-width of the emission calculated with these fields included is 11 μm, which is 2.5 times larger than simulated without them, but still a factor 6 smaller than measured.

The hot electrons which pass the magnetic field are deflected and enter the solid at shallow angles. This provides an explanation for the increased yield compared to the PIC-MC simulations (Fig. 9). It could also explain observations made by other groups, such as the angular spread [14], anomalously low penetration depths [42], and unexpected low temperatures [43,44] of the hot electrons.

The crucial point in our estimate of self-induced fields is the presence of a magnetic field, generated by prepulses, which reflects a large portion of the hot electrons. The strength of this field is related to the prepulse parameters via the temperature and density gradients of the produced preplasma. We found a scaling of the field strength proportional to the square root of the prepulse intensity and to the reciprocal of the focus diameter. This scaling implies that the magnetic field quickly decreases when the laser is defocused.

The discrepancies between modeling and experiment point to other (or much stronger) self-induced fields than those used in the above estimate. Possible candidates are the magnetic fields generated due to the space and time dependence of the ponderomotive force [45], by the surface plasma electrons acquiring a net lateral momentum due to the oblique incidence of the laser beam [46], and the resistive electric field and magnetic field set up by the hot electron current [47,48]. Also, experiments point to the importance of electric fields inside the bulk material on the transport of the hot electrons [49–51]. Moreover, the generation and propagation phases of the hot electrons cannot be completely separated as was done in our modeling. Clearly, more sophisticated two- and three-dimensional modeling is needed to identify the important electric- and magnetic-field generation mechanisms and provide a self-consistent picture of hot electron transport in relativistic, femtosecond laser interactions with high-density targets.

VI. CONCLUSIONS

We have measured the spatial distribution of the Kα emission from femtosecond laser-produced Ti plasmas with two-dimensional 6-μm spatial resolution. We found qualitatively different spatial structures of the Kα emission for high and low laser intensities (above and below 10^{17} W/cm^2). At low intensities the Kα emission consists of one broad peak, while at high intensities the central Kα peak is surrounded by a large halo of weak Kα emission, which delivers two-thirds of the total emission. For a laser intensity of 7×10^{18} W/cm^2 the Kα radiation originates from an area with a total diameter of 400 μm compared to a laser focus size of 3 μm. The peak Kα emission (coming from the source center) does not increase with increasing laser intensity, or even decreases.

The experimental findings were compared with the predictions of a PIC-MC simulation model, which calculates the spatial structure of the Kα emission resulting from the physics of laser absorption and hot electron scattering in the solid. The comparison shows that the physics included in the model is sufficient to explain the spatial Kα distribution at low laser intensities. For high intensities, the measured peak Kα emission is only one-third of that expected from the model and the observed Kα halo is not reproduced by the simulations. Both observations indicate the presence of mechanisms, not included in the model, which redirect the hot electrons away from the laser focus towards the fringes.

An estimate of the hot electron trajectories in self-induced fields suggests that the electrons are reflected in the focus center by a thermoelectric magnetic field generated by prepulses, while the large extension of the Kα source may be due to the lateral component of the ponderomotive force.

ACKNOWLEDGMENTS

The authors wish to thank O. Wehrhan and T. Haertling for the support in preparing the experiments. This work was supported by the German Science Council (DFG), Contract No. GI 300/1-2, and by the BMBF, Contract No. 13N 7921.

[1] P. Gibbon and E. Förster, Plasma Phys. Controlled Fusion **38**, 769 (1996).

[2] A. Rousse, P. Audebert, J.P. Geindre, F. Falliès, J.C. Gauthier, A. Mysyrowicz, G. Grillon, and A. Antonetti, Phys. Rev. E **50**, 2200 (1994).

[3] J. Yu, Z. Jiang, and C. Kieffer, Phys. Plasmas **6**, 1318 (1999).

[4] C. Reich, P. Gibbon, I. Uschmann, and E. Förster, Phys. Rev. Lett. **84**, 4846 (2000).

[5] T. Feurer, A. Morak, I. Uschmann, C. Ziener, H. Schwoerer, C. Reich, P. Gibbon, E. Förster, R. Sauerbrey, K. Ortner, and C.R. Becker, Phys. Rev. E **65**, 016412 (2002).

[6] K. Sokolowski-Tinten, C. Blome, C. Dietrich, A. Tarasevitch, M. Horn von Hoegen, D. von der Linde, A. Cavalleri, J. Squier, and M. Kammler, Phys. Rev. Lett. **87**, 225701 (2001).

[7] A. Rousse *et al.*, Nature (London) **410**, 65 (2001).

[8] C. Rischel, A. Rousse, I. Uschmann, P.-A. Albouy, J.-P. Geindre, P. Audebert, J.-C. Gauthier, E. Förster, J.-L. Martin, and A. Antonetti, Nature (London) **390**, 490 (1997).

[9] S. Svanberg, J. Larsson, A. Persson, and C.-G. Wahlström, Phys. Scr. **49**, 187 (1994).

[10] C. Tillman, I. Mercer, S. Svanberg, and K. Herrlin, J. Opt. Soc. Am. B **13**, 209 (1996).

[11] B. Soom, H. Chen, Y. Fisher, and D.D. Meyerhofer, J. Appl. Phys. **74**, 5372 (1993).

[12] D.C. Eder, G. Pretzler, E. Fill, K. Eidmann, and A. Saemann, Appl. Phys. B: Lasers Opt. **B70**, 211 (2000).

[13] T. Guo, C. Spielmann, B. Walker, and C. Barty, Rev. Sci. Instrum. **72**, 41 (2001).

[14] G. Pretzler, T. Schlegel, E. Fill, and D. Eder, Phys. Rev. E **62**, 5618 (2000).

[15] K.B. Wharton, S.P. Hatchett, S.C. Wilks, M.H. Key, J.D. Moody, V. Yanovsky, A.A. Offenberger, B.A. Hammel, M.D. Perry, and C. Joshi, Phys. Rev. Lett. **81**, 822 (1998).

[16] H. Schwoerer, P. Gibbon, S. Düsterer, R. Behrens, C. Ziener, C. Reich, and R. Sauerbrey, Phys. Rev. Lett. **86**, 2317 (2001).

[17] Z.-M. Sheng, Y. Sentoku, K. Mima, J. Zhang, W. Yu, and J. Meyer-ter-Vehn, Phys. Rev. Lett. **85**, 5340 (2000).

[18] H. Ruhl, Y. Sentoku, K. Mima, K.A. Tanaka, and R. Kodama, Phys. Rev. Lett. **82**, 743 (1999).

[19] Y. Sentoku, H. Ruhl, K. Mima, R. Kodama, K.A. Tanaka, and Y. Kishimoto, Phys. Plasmas **6**, 2855 (1999).

[20] I. Uschmann, P. Gibbon, D. Klöpfel, T. Feurer, E. Förster, P. Audebert, J.-P. Geindre, J.-C. Gauthier, A. Rousse, and C. Rischel, Laser Part. Beams **17**, 671 (1999).

[21] A.G. Zhidkov, A. Sasaki, I. Fukumoto, and T. Tajima, Phys. Plasmas **8**, 3718 (2001).

[22] R. Fabbro and P. Mora, Phys. Lett. **90A**, 48 (1982).

[23] D.W. Forslund and J.U. Brackbill, Phys. Rev. Lett. **48**, 1614 (1982).

[24] M.D.J. Burgess, B. Luther-Davies, and K.A. Nugent, Phys. Fluids **28**, 2286 (1985).

[25] T. Feurer, E. Förster, P. Gibbon, A. Morak, R. Sauerbrey, and I. Uschmann, in *Applications of High Field and Short Wavelength Sources VIII* (OSA, Washington, DC, 1999), pp. 108–110.

[26] E. Förster, K. Gäbel, and I. Uschmann, Laser Part. Beams **9**, 135 (1991).
[27] C. Reich, Ph.D. thesis, Friedrich Schiller Universität Jena, 2002, published online at http://www.db-thueringen.de/dissOnline/FSU_Jena_Reich_Christian
[28] P. Gibbon and A.R. Bell, Phys. Rev. Lett. **68**, 1535 (1992).
[29] P. Gibbon, A.A. Andreev, E. Lefebvre, G. Bonnaud, H. Ruhl, J. Delettrez, and A. Bell, Phys. Plasmas **6**, 947 (1999).
[30] C. Ziener *et al.*, Phys. Rev. E **65**, 066411 (2002).
[31] Y.T. Li *et al.*, Phys. Rev. E **64**, 046407 (2001).
[32] G. Malka *et al.*, Phys. Rev. Lett. **79**, 2053 (1997).
[33] K. Estabrook and W.L. Kruer, Phys. Rev. Lett. **40**, 42 (1978).
[34] C.E. Dick, A.C. Lucas, J.M. Motz, R.C. Placious, and J.H. Sparrow, J. Appl. Phys. **44**, 815 (1973).
[35] M. Dirksmöller, O. Rancu, I. Uschmann, P. Renaudin, C. Chenais-Popovics, J. Gauthier, and E. Förster, Opt. Commun. **118**, 379 (1995).
[36] S. Bastiani, A. Rousse, J.P. Geindre, P. Audebert, C. Quoix, G. Hamoniaux, A. Antonetti, and J.-C. Gauthier, Phys. Rev. E **56**, 7179 (1997).
[37] A. Morak, I. Uschmann, C. Ziener, T. Feurer, H. Schwoerer, E. Förster, and R. Sauerbrey, Appl. Phys. B (to be published).
[38] F. Ewald, H. Schwoerer, and R. Sauerbrey, Europhys. Lett. **60**, 710 (2002).
[39] J.A. Stamper, K. Papadopoulos, R.N. Sudan, S.O. Dean, and E.A. McLean, Phys. Rev. Lett. **26**, 1012 (1971).
[40] J.P. Christiansen, D.E.T.F. Ashby, and K.V. Roberts, Comput. Phys. Commun. **7**, 271 (1974).
[41] M.G. Haines, Phys. Rev. Lett. **78**, 254 (1997).
[42] T. Feurer, W. Theobald, R. Sauerbrey, I. Uschmann, D. Altenbernd, U. Teubner, P. Gibbon, E. Förster, G. Malka, and J.L. Miquel, Phys. Rev. E **56**, 4608 (1997).
[43] U. Teubner *et al.*, Phys. Rev. E **54**, 4167 (1996).
[44] Z. Jiang, J.C. Kieffer, J.P. Matte, M. Chaker, O. Peyrusse, D. Gilles, G. Korn, A. Maksimchuk, S. Coe, and G. Mourou, Phys. Plasmas **2**, 1702 (1995).
[45] R.N. Sudan, Phys. Rev. Lett. **70**, 3075 (1993).
[46] F. Brunel, Phys. Fluids **31**, 2714 (1988).
[47] A.R. Bell, J.R. Davies, S. Guérin, and H. Ruhl, Plasma Phys. Controlled Fusion **39**, 653 (1997).
[48] J.R. Davies, A.R. Bell, M.G. Haines, and S.M. Guérin, Phys. Rev. E **56**, 7193 (1997).
[49] F. Pisani *et al.*, Phys. Rev. E **62**, 5927 (2000).
[50] T.A. Hall *et al.*, Phys. Rev. Lett. **81**, 1003 (1998).
[51] D. Batani *et al.*, Phys. Rev. E **61**, 5725 (2000).